Available online at www.sciencedirect.com
ScienceDirect
Journal of Power Sources 163 (2007) 671–678
JOURNAL OF POWER SOURCES
www.elsevier.com/locate/jpowsour

Thin film Pt/TiO_2 catalysts for the polymer electrolyte fuel cell

M. Gustavsson [a,b], H. Ekström [c], P. Hanarp [a,b,*], L. Eurenius [a,b], G. Lindbergh [c], E. Olsson [b], B. Kasemo [a,b]

[a] *Competence Centre for Catalysis, Chalmers University of Technology, SE-412 96 Göteborg, Sweden*
[b] *Department of Applied Physics, Chalmers University of Technology, SE-412 96 Göteborg, Sweden*
[c] *Department of Chemical Engineering and Technology, Applied Electrochemistry, Kungl Tekniska Högskolan, SE-100 44 Stockholm, Sweden*

Received 13 June 2006; received in revised form 29 August 2006; accepted 4 October 2006
Available online 13 November 2006

Abstract

Thin film Pt/TiO_2 catalysts are evaluated in a polymer electrolyte electrochemical cell. Individual thin films of Pt and TiO_2, and bilayers of them, were deposited directly on Nafion membranes by thermal evaporation with varying deposition order and thickness (Pt loadings of 3–6 μg cm^{-2}). Structural and chemical characterization was performed by transmission electron microscopy (TEM), and X-ray photoelectron spectroscopy (XPS). Oxygen reduction reaction (ORR) polarization plots show that the presence of a thin TiO_2 layer between the platinum and the Nafion increases the performance compared to a Pt film deposited directly on Nafion. Based on the TEM analysis, we attribute this improvement to a better dispersion of Pt on TiO_2 compared to on Nafion and in addition, substantial proton conduction through the thin TiO_2 layer. It is also shown that deposition order and the film thickness affects the performance.

Keywords: Fuel cells; Polymer electrolyte; Oxygen reduction; Electrocatalyst; Pt; TiO_2

1. Introduction

The polymer electrolyte fuel cell (PEMFC) is a promising energy conversion system for transportation and portable power applications [1], with a high power density and potential for zero emissions. However, for a widespread commercial use of fuel cells there is a need to lower the overall fuel cell cost, and to improve the performance and durability of fuel cell components such as the proton conducting membrane, the bipolar plates and the catalyst. The rare noble metal Pt is the most commonly used metal in fuel cell catalysts. To lower the over all fuel cell cost, there is a need to significantly reduce the amount of Pt catalyst in the electrodes [2].

Conventional catalysts are fabricated by first depositing catalyst material onto a high surface area carbon nanoparticle support. The carbon-supported catalysts are then mixed with Nafion solution to ink, and further deposited on Nafion membranes to form the electrodes [3]. The typical size scales in the electrode are 2–5 nm for the Pt catalyst particles, 10–30 nm for the carbon support, and 10–50 μm for the whole electrode layer. The highly heterogeneous structure of the porous electrode introduces limitations in mass transport of reacting species as well as Ohmic resistances. Although there have been extensive efforts to find the best fabrication procedures and morphologies of porous electrodes, by varying for example, Pt particle size, Nafion/Pt/C mixing ratio [2,4–7] and electrode configuration [8], the detailed knowledge of the mechanisms that take place inside the porous electrodes during oxygen reduction is still insufficient.

Catalysts with more well-defined structural arrangements can be fabricated on planar glassy carbon substrate by nanofabrication [9–11] or microstructuring [12], similar to what has been done to mimic various catalysts for normal heterogeneous catalysis [13–16]. These catalysts can be used as model systems (e.g. representing a thin cross-section of a porous electrode) for studying the structural influence of processes at the catalyst/support interface and also for mechanistic studies in both liquid electrolyte and in a more fuel cell like environment. A

* Corresponding author at: Competence Centre for Catalysis, Chalmers University of Technology, SE-412 96 Göteborg, Sweden. Tel.: +46 31 772 2958; fax: +46 31 772 3134.
E-mail address: per.hanarp@fy.chalmers.se (P. Hanarp).

0378-7753/$ – see front matter © 2006 Elsevier B.V. All rights reserved.
doi:10.1016/j.jpowsour.2006.10.005

recent approach to prepare and evaluate low loading catalysts in a fuel cell environment, eliminating the limitations present in a porous structure, is to deposit metal thin films directly on the gas backing or on the Nafion membrane [17–23].

A large range of alternative catalyst materials containing less or no Pt, have been evaluated for oxygen reduction in the PEMFC [24]. Conventional porous electrodes containing Pt–TiO_x/C and Pt–WO_3/C have been investigated [25,26], and an improved fuel cell performance was seen with the addition of the oxides. The Pt/TiO_x system has also been further investigated by depositing Pt on a TiO_2 support using electrodeposition [27,28] or by vacuum deposition techniques [29].

In the present work we use thin Pt/TiO_2 bi-layer film catalysts as a model system to study the influence of the interfacial structure of the metal oxide and the Pt–Nafion/oxygen interface. The model catalysts are fabricated by thermal evaporation of thin Pt and/or TiO_2 films with total thickness of 3–6 nm directly on Nafion 117 membranes. This corresponds to electrode Pt loadings of 3–6 $\mu g\,cm^{-2}$. The thin film catalysts are used as working electrodes for studying oxygen reduction as well as cyclic voltammetry behaviour in nitrogen in a laboratory fuel cell. On the basis of the combined electrochemical measurements, X-ray photoelectron spectroscopy (XPS) characterization and transmission electron microscopy (TEM) data of the thin films, we discuss the observed large variations in oxygen reduction performance, when the amount of material and the deposition order (Pt followed by TiO_2 or reverse) were varied.

2. Experimental

2.1. Materials preparation

Commercial double-sided membrane-electrode assembly (MEA) material, used as counter/reference electrodes, was purchased from Gore Technologies (Gore PRIMEA MEA Cleo Series 5620, membrane thickness 35 um, Pt loading 0.6 $mg\,cm^{-2}$ on one side, 0.4 $mg\,cm^{-2}$ on the other side). A sheet of this MEA material was placed on a 95 °C hot bed and spray-brushed with Nafion solution on the 0.6 $mg\,cm^{-2}$ side, to create a thin Nafion layer (around 1.5 $mg\,cm^{-2}$) on top of the electrode. The MEA sheet was cut into 35 mm × 35 mm pieces. Then, the sprayed pieces were all immersed into 0.1 M H_2SO_4 for more than 24 h at room temperature, then thoroughly rinsed in MilliQ water, stored in MilliQ water for more than 24 h and finally dried in an oven at 60 °C for 30 min.

Sigracet 21 BC gas backings for the working electrode side were purchased from SGL Technologies GmbH and cut into 15 mm radius pieces. Carbel CL carbon cloth material for the counter electrode side was purchased from Gore Technologies and cut into 14 mm radius pieces. Both gas diffusion materials contained microporous layers facing the electrodes.

Nafion membranes (Nafion 117, Aldrich) were cut into 45 mm × 45 mm pieces and cleaned by, boiling in 3% H_2O_2 for 1 h, boiling in 0.1 M H_2SO_4 for 1 h, and finally boiling in three successive baths of Milli-Q water for 1 h each and then dried under flowing nitrogen gas. Single and/or bi-layer Pt and Ti films were deposited on the Nafion membranes by thermal evaporation in vacuum (AVAC HVC-600, 10^{-6} mbar); the thickness was measured with a quarts crystal microbalance sensor located in the chamber. Prior to film deposition the membrane surface was cleaned by oxygen plasma treatment (PE/RIE, 50W) for 2 min. Bi-layer films were fabricated by deposition of 1.5 nm and 3 nm thick films of Ti and Pt in different orders. The Ti films were oxidised to natural TiO_2 films when venting to atmospheric pressure.

The samples with these thin catalyst layers are named as for example, 3 nmPt/3 nmTiO_2/Nafion where, in this example, the Pt layer is on top facing the gas side and the TiO_2 is underneath facing the Nafion.

2.2. Electrochemical cell setup and measurement procedure

Before final mounting, the Nafion painted electrode side of the commercial MEAs was hot pressed to the non-catalysed side of the Nafion 117 membranes, at 129 °C for 30 s at 1 MPa. (Note: only one side of the GORE MEA is operating in the cell, the Nafion painted side gets electrochemically inactive. The choice of counter electrode was in this case for reproducibility and convenience. In principle any counter electrode with a large platinum area may be used.) The resulting double membrane-electrode assembly was mounted in homebuilt laboratory PEEK (polyether-etherketone) fuel cell [30], sandwiched between the gas backings in contact with circular 15 mm radius graphite current collectors with spirally formed gas channels, gas entering at the centre. The cell was clamped together by applying a force of 380 N over the current collectors. A schematic of the measurement setup can be seen in Fig. 1.

The fuel cell was connected to a PAR 273A potentiostat, with the thin film catalyst side of the Nafion membrane as working electrode (WE) and the commercial non-Nafion-sprayed MEA side as combined counter and reference (CE/RE) electrode. The cell was heated to 80 °C. Gases were fed in excess rate into the centre of the current collectors; the WE-side was fed with nitrogen or oxygen at a rate of around 1 ml s^{-1} and 0.5 ml s^{-1}, respectively, the CE/RE with 5% hydrogen in argon at a rate of around 2 ml s^{-1}. These gas flows of hydrogen and oxygen correspond to stoichiometric ratios of more than 10:1 for the highest current densities in this study. All gases were humidified by bubbling the gas through heated humidifiers at 85 °C from Fuel Cell Technologies Inc.

Due to the low currents at the CE/RE in combination with the very high surface area for this porous electrode, the CE/RE is not supposed to be polarised during the experiment. In order to present the cathode potential versus a 100% hydrogen anode (denoted RHE), all measured potentials have been corrected for the 45.5 mV shift (calculated from Nernst equation) due to the lower 5% partial pressure of hydrogen in argon used.

The cell was first left to equilibrate at open circuit for 90 min with nitrogen at the WE. After recording 50 cyclic voltammograms at 200 mV s^{-1} between 0.1 and 1.15 V versus RHE, the gas at the WE was changed to oxygen and left to equilibrate for 15 min. In oxygen, polarization data was obtained by repeating the following scan/hold scheme five times; 15 min at open cir-

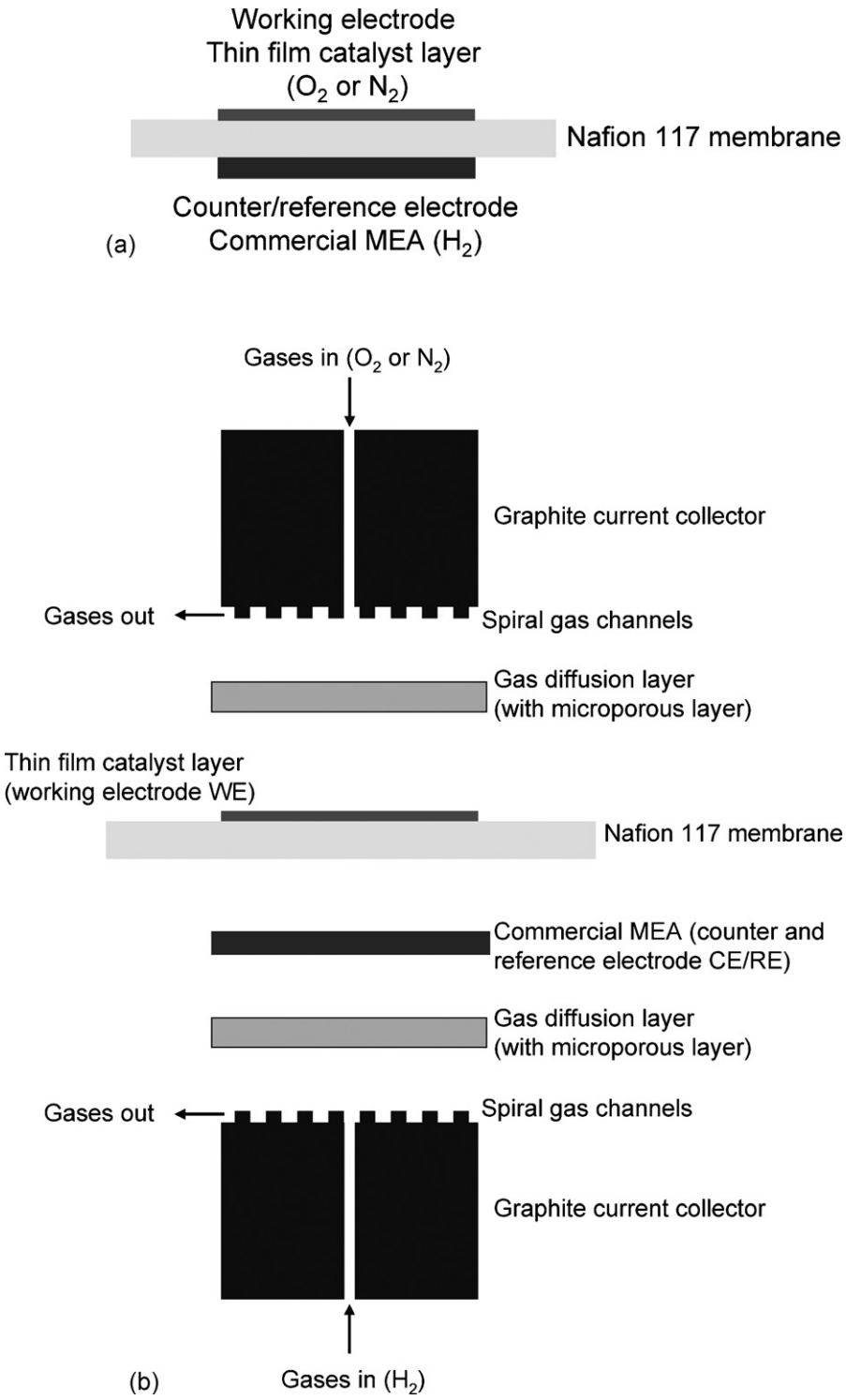

Fig. 1. Schematic of the working and counter/reference electrode assembly. (a) Sideview of the MEA setup used in this work including thin film catalyst layer used as working electrode, Nafion 117 membrane and commercial MEA used as counter/reference electrode. (b) Detailed sideview of the cell assembly including graphite current collectors, gas diffusion layers (with microporous layers), thin film catalyst layer used as working electrode WE, Nafion 117 membrane and commercial MEA used as counter and reference electrode CE/RE. The cell assembly has a circular symmetry, with 15 nm radius.

cuit followed by a slow cathodic $-1\,\mathrm{mV\,s^{-1}}$ step scan down to 0.5 V versus RHE, then a 15 min potential hold at 0.5 V versus RHE and finally a slow anodic $1\,\mathrm{mV\,s^{-1}}$ step scan returning to the open circuit potential.

All measurements were repeated with at least two separate samples for each sample type, with good agreement between these samples. All currents reported here (as $\mathrm{A\,cm^{-2}}$) refers to the geometrical current density.

2.3. Materials morphology and chemistry characterization

The morphology of the thin film catalysts was characterized by transmission electron microscopy (Phillips CM200 TEM). Simultaneously, with the thin film deposition on the Nafion membrane the corresponding films were also deposited on TEM-windows. The TEM-windows are made of Si_3N_4 and enable a direct TEM imaging of the films without further sample preparation [31]. To validate that the films deposited on TEM-windows are representative for the case of films deposited on Nafion, a corresponding film was also deposited on a Nafion coated TEM-grid for one sample type (not shown here). The two samples showed good agreement. For practical reasons, film deposition on TEM-windows was then used throughout the study.

The chemical characterization of the thin film catalysts was performed in an XPS system (Perkin Elmer PHI 5000C ESCA system) employing 350 W Mg Kα radiation and a 45° take-off angle. The electron energy spectra were analyzed by Multipak software and the results are presented as surface elemental composition (atomic %) for the main elements on the electrode surfaces.

3. Results

3.1. Electrochemical evaluation

Fig. 2 shows the oxygen reduction reaction ORR polarization plots for Pt/TiO_2 films with a constant total film thickness of 3 nm. As can be seen, 3 nmPt/Nafion sample shows the best performance while 3 nmTiO_2/Nafion has poor activity. For the 1.5 + 1.5 nm bi-layer films the sample with a TiO_2 film deposited closest to the Nafion (1.5 nm Pt/1.5 nm TiO_2/Nafion) has significantly higher activity than the reversed order of deposition (1.5 nm TiO_2/1.5 nm Pt/Nafion). When depositing a 1.5 nm Pt film on a TiO_2 coated Nafion the ORR activity approaches the activity for a bare 3 nm Pt film.

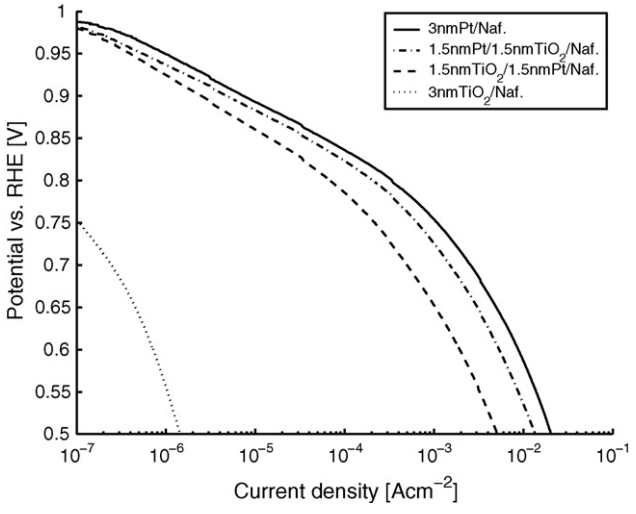

Fig. 2. Oxygen reduction polarization plots for Pt/TiO_2 films with a constant total film thickness (3 nm in total). The thin catalyst film activities rank as 3 nm Pt/Nafion > 1.5 nm Pt/1.5 nm TiO_2/Nafion > 1.5 nm TiO_2/1.5 nm Pt/Nafion > 3 nm TiO_2/Nafion. The polarization data is obtained by a step scan (-1 mV s^{-1}) from the open circuit potential down to 0.5 V, at 80 °C. Gases were humidified to 100% relative humidity.

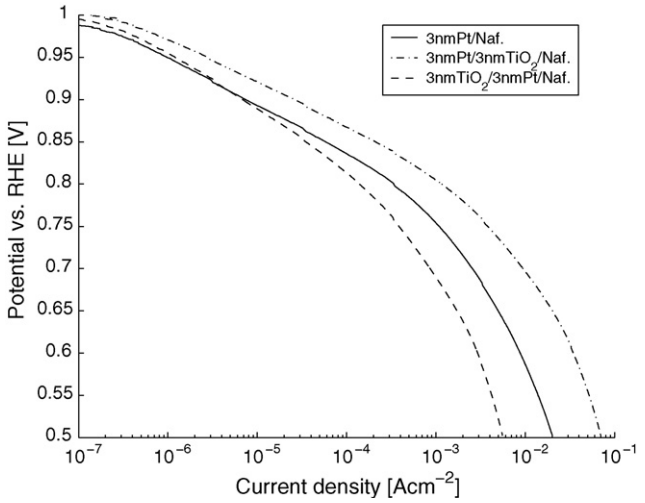

Fig. 3. Oxygen reduction polarization plot for Pt/TiO_2 films with a constant Pt-layer thickness (3 nm Pt). The thin catalyst film activities rank as 3 nm Pt/3 nm TiO_2/Nafion > 3 nm Pt/Nafion > 3 nm TiO_2/3 nm Pt/Nafion. The polarization data is obtained by a step scan (-1 mV s^{-1}) from the open circuit potential down to 0.5 V, at 80 °C with humidified gases at 100% relative humidity.

Fig. 3 shows the ORR polarization plots for Pt/TiO_2 films with a constant Pt film thickness of 3 nm. Here the activity of the films ranks as 3 nm Pt/3 nm TiO_2/Nafion > 3 nm Pt/Nafion > 3 nm TiO_2/3 nm Pt/Nafion. Thus, in this experimental setup the performance of 3 nm Pt film has been improved by adding a 3 nm TiO_2 film on the Nafion membrane prior the deposition of the Pt layer. The reverse order with Pt closest to the Nafion membrane and TiO_2 on top shows significantly lower performance.

Between 0.95 and 0.85 V versus RHE, a linear Tafel region was observed for all Pt-containing samples in Figs. 2 and 3. The value of the slope, given in Table 1, was around 55 mV $decade^{-1}$ for the samples with Pt facing the gas backing, i.e., the "gas phase", and significantly higher (65 mV $decade^{-1}$) for the samples with TiO_2 facing the gas backing.

Figs. 4 and 5 show the cyclic voltammograms in nitrogen gas for the samples of Figs. 2 and 3 respectively. The electrochemically active surface area of Pt was obtained by integrating the current of the hydrogen desorption peaks in the positive sweep direction and dividing that value with 220 μC cm^{-2}. Results from the electrochemical evaluation above are summarized in Table 1.

From the results above it is evident that the geometry of the bi-layer films, i.e., the specific Pt/TiO_2 interface with Nafion/oxygen, is an important factor for the performance. The samples with Pt facing the gas backing side, i.e., the "gas phase", show highest activity, whereas the samples with TiO_2 on top are less active. The active surface area for the different samples, from CV measurements, correlates well with the oxygen reduction currents at 0.85 V versus RHE.

Table 1
Summary of the electrochemical evaluation on all Pt/TiO_2 films presented in Figs. 2–5

Sample	A_{Pt} ($cm^2 Pt\ cm^{-2}$)	$I_{(0.85\,V)}$ ($\times 10^{-5}$ A cm^{-2})	$I_{(0.65\,V)}$ ($\times 10^{-5}$ A cm^{-2})	$b_{(0.95–0.85\,V)}$ (mV $decade^{-1}$)
3 nm Pt/Nafion	0.07	5.9	500	56
3 nm Pt/3 nm TiO_2/Nafion	0.38	22	2000	53
1.5 nm Pt/1.5 nm TiO_2/Nafion	0.06	3.7	300	54
3 nm TiO_2/Nafion	–	0.00049	0.045	–
3 nm TiO_2/3 nm Pt/Nafion	0.06	3.5	170	68
1.5 nm TiO_2/1.5 nm Pt/Nafion	0.02	1.5	100	64

Columns from the left to right: electrochemically active surface area of Pt based on the hydrogen desorption charge, oxygen reduction current at 0.85 V and 0.65 V, respectively, vs. RHE and Tafel-slope of the E–log i polarization data for oxygen reduction in the linear region between 0.95 and 0.85 V vs. RHE. *Note*: A cm^{-2} refers to the geometrical current density.

3.2. Materials morphology and chemistry characterization

Fig. 6 shows TEM microscopy images of all Pt/TiO_2 films in the study. All films are deposited on TEM-windows. As can be seen for the single layer films in Fig. 6(a and d), TiO_2 forms a more well spread film than Pt on bare Nafion. For the images containing both Pt and TiO_2, Fig. 6(b–c and e–f), the contrast has to be interpreted with some caution. Comparing pure Pt and TiO_2 films it is clear that Pt gives more contrast. Jump ratio images on mixed TiO_2 films obtained by energy filtering (not shown here) indicate that Ti is present also in the spaces between the Pt grains. All film morphologies can be described as network structure (structures where originally individual grains have in most cases coalesced with neighboring grains, forming a continuous structure), with a projected area coverage of 70–90%. The TiO_2 film forms a well spread film in all cases, while the Pt film formation depends on the deposition order. A Pt film deposited on top of TiO_2 is more well-spread with slightly increased projected surface area compared to a Pt film directly on the Nafion (see for example, Fig. 6 (a and e)).

The chemical composition of the samples was characterized by XPS measurements. In Fig. 7, the XPS spectra of 3 nm Pt/Nafion, 3 nm Pt/3 nm TiO_2/Nafion and 3 nm TiO_2/3 nm Pt/Nafion samples can be seen. The XPS data from all Pt/TiO_2 films are summarized in Table 2. As expected, there is a layering of the fabricated bi-layer films with the two materials situated on top of the other, rather than in a mixture. When Pt is on top, a large Pt signal and only trace amounts of Ti is seen, and vice versa. Also, the exposed area of Nafion (using the fluorine signal as an indication) is decreased for the highest coverage films, 3 nm Pt/3 nm TiO_2/Nafion and 3 nm TiO_2/Nafion, confirming the microscopy data in Fig. 6. The fact that the Pt signal is larger for the 3 nm Pt/3 nm TiO_2/Nafion than for 3 nm Pt/Nafion, is in agreement with the conclusion from TEM data that Pt spreads better on TiO_2 than on bare TEM window or Nafion.

The chemical shift in the Ti peak is in agreement with TiO_2. In the electrochemical experiments, the oxidation state of a TiO_x film depends on the pH and potential range. For the potential window between 1.2 and 0 V versus RHE in an acid environment, the most stable oxidation state is TiO_2.

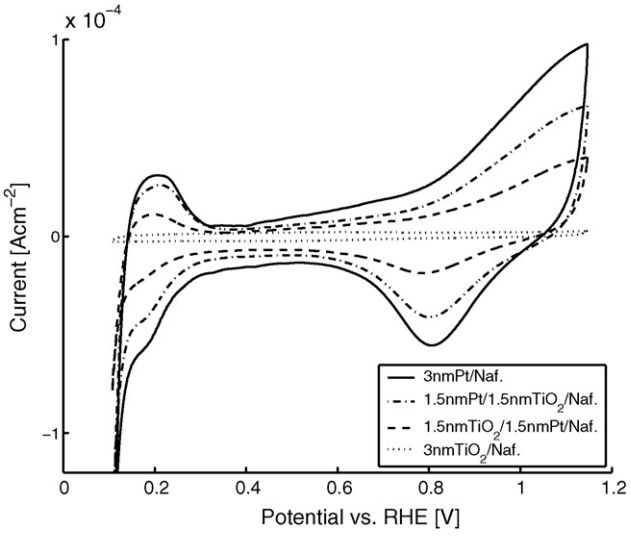

Fig. 4. Cyclic voltammograms in N_2 for Pt/TiO_2 films for with a constant total film thickness (3 nm in total). Sweep rate: 200 mV s^{-1}.

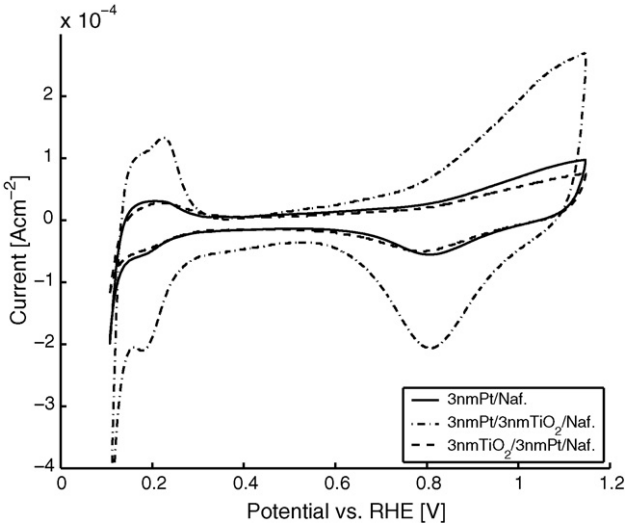

Fig. 5. Cyclic voltammograms in N2 for Pt/TiO_2 films for films with a constant Pt-layer thickness (3 nm Pt). Sweep rate: 200 mV s^{-1}.

4. Discussion

Our results show that the presence of TiO_2 can either increase or decrease the ORR performance of a given amount of Pt, depending on deposition order of the thin films. As seen in Table 1, the pre-deposited TiO_2 film increases the electrochemically active area of later deposited Pt, which also increases the

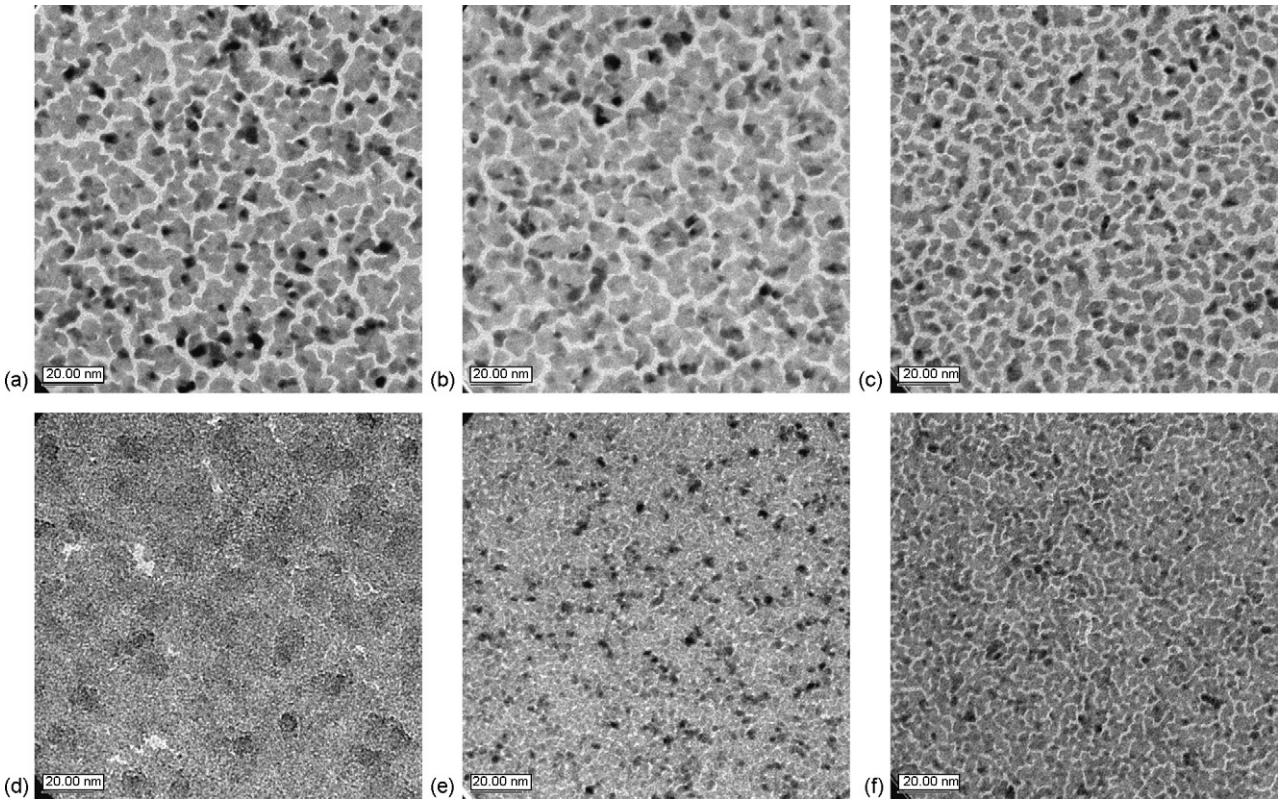

Fig. 6. TEM microscopy images of Pt, TiO_2 and Pt/TiO_2 samples; (a) 3 nm Pt/TEM, (b) 3 nm TiO_2/3 nm Pt/TEM, c) 1.5 nm TiO_2/1.5 nm Pt/TEM, (d) 3 nm TiO_2/TEM, (e) 3 nm Pt/3 nm TiO_2/TEM, (f) 1.5 nm Pt/1.5 nm TiO_2/TEM. All films are deposited on TEM-windows.

activity of the catalytic layer. The increase in area is seen in the TEM images in Fig. 6 (a and e); the Pt films deposited on top of TiO_2 are more spread than the Pt films deposited on bare Nafion. Thus, the main effect of the TiO_2 under layer is attributed to a better dispersion of Pt on TiO_2 compared to Nafion, creating a larger surface area of Pt, on TiO_2, for the same Pt mass. However, we cannot exclude that there is additionally a more subtle cooperative electro-catalytic effect, like strong metal support interaction SMSI [32] at the rim of Pt grains on TiO_2.

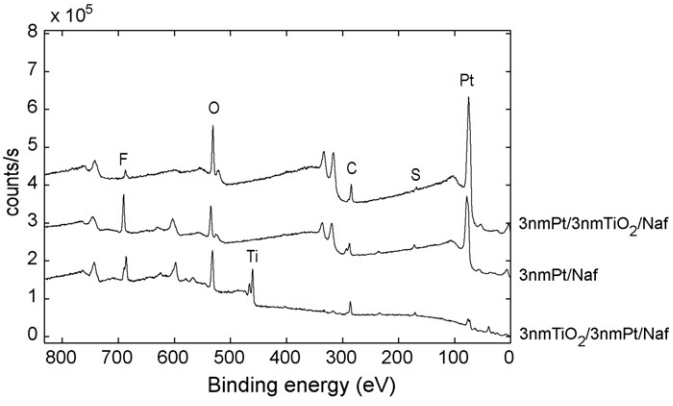

Fig. 7. XPS spectra of the 3 nm Pt/Nafion, 3 nm Pt/3 nm TiO_2/Nafion and 3 nm TiO_2/3 nm Pt/Nafion samples. Data was obtained using 350 W Mg Kα radiation and a 45° take-off angle. The primary peaks of each element are indicated. Comparison of the Pt peaks, indicate the strong layering of the thin films with large signal when Pt is deposited on top and small signal when Pt is underneath the TiO_2. A summary of the XPS analysis for all samples is given in Table 2.

Characterization by XPS indicates a clear layering of the materials. When the TiO_2 layer is at the bottom, the Pt film has a large fraction of its surface in contact with the gas backing side, i.e., the "gas phase", and only a minimum contact with Nafion. In Fig. 6(d), it can be seen that the 3 nm TiO_2 film is fairly even and produces a large coverage. However, it still seems that proton transport through the TiO_2 layer is good enough over these distances not to hamper the oxygen reduction performance. It is known that small ions, such as H^+ and Li^+, are able to diffuse through the TiO_2 structure [33]. The very similar Tafel slopes for Pt on bare Nafion compared to the other samples with Pt on top of TiO_2 indicate no significant differences regarding local species transport, electronic contact or rate determining step in the electrochemical reaction.

When depositing TiO_2 on top of Pt we see a completely different effect, this lowers activity but not the active surface area to any larger extent. Returning to Table 1, we see that the addition of a 3 nm TiO_2 layer on top of 3 nm Pt has little effect on the electrochemically active Pt area, but oxygen reduction currents are lowered considerably. Especially for lower potentials the Tafel slopes are increased when having TiO_2 on top. This could be due to blocking of oxygen and water transport to and from the active sites, but also due to poor local electron conduction of TiO_2.

Comparing the film morphologies in Fig. 6 with the surface areas in Table 1, we can see that the electrochemically accessible

Table 2
Results of XPS analysis, atomic% of the present elements for all films in the study

Sample	Pt (atomic%)	Ti (atomic%)	F (atomic%)	S (atomic%)	C (atomic%)	O (atomic%)
3 nm Pt/Nafion	12	–	21	4.0	35	28
3 nm Pt/3 nm TiO_2/Nafion	19	0.1	8.3	1.8	33	38
1.5 nm Pt/1.5 nm TiO_2/Nafion	10	0.1	22	2.0	37	29
3 nm TiO_2/Nafion	–	13	16	3.1	25	43
3 nm TiO_2/3 nm Pt/Nafion	1.6	13	21	3.3	22	40
1.5 nmTiO_2/1.5 nm Pt/Nafion	3.6	7.1	25	3.5	26	35

surface areas are lower than the geometrical film coverage. This is often seen in fuel cell experiments [34]. In our experimental setup, this might indicate that the electrical contact of the thin films with the gas backing is not complete. For best electrical contact, we have chosen a gas backing with a microporous layer.

The results that additional TiO_2 can improve the accessible area and activity of a given amount of Pt is in agreement with previous studies on porous electrodes, even though both fabrication methods and final structures are vastly different. In studies on conventional porous Pt-catalyst electrodes, with TiO_2 or WO_3 nanoparticles added to the electrode, an increase in both Pt surface area and activity was seen [25,26]. The cause of the enhanced activities was suggested to be a combination of the addition of more active sites at the Pt-metal oxide interface and to spill over effects by surface diffusion. In RDE experiments a specific increase in activity for a few Pt–Ti (non-oxidised) sites has also been observed [28]. While our results cannot exclude contributions from any of these proposed mechanisms, the enhancement in our study is more likely to be caused by the increased Pt area when deposited on TiO_2 and proton conduction through the thin TiO_2 layer.

5. Conclusion

We have studied thermally evaporated thin Pt/TiO_2 films, used as cathodes in the polymer electrolyte fuel cell. The results indicate that TiO_2 can both increase (+) or decrease (−) the performance of a PEFC electrode, depending on geometrical placement. We interpret our results as being related to the following material properties of TiO_2: good proton conduction over nm size scale (+), ability to stabilize deposition of Pt (+), poor electrical conduction of TiO_2 over nm size scale (−) and no conduction of gas phase O_2 in solid TiO_2 (−). Thus, in our model experiments we find an increase in performance when TiO_2 is placed in between Pt and Nafion, while a decreased performance when TiO_2 is placed in between Pt and the carbon electrical conductor. We suggest that incorporation of TiO_2 in real PEFC porous electrodes, using the suggested "design guidelines" in this work, should be beneficial for performance and stability of the electrode materials.

Acknowledgments

This study has been performed within the Competence Centre for Catalysis, which is hosted by Chalmers University of Technology and financially supported by the Swedish Energy Agency and the member companies: AB Volvo, Volvo Car Corporation, Scania CV AB, GM Powertrain Sweden AB, Haldor Topsøe A/S, Perstorp Specialty Chemicals AB and The Swedish Space Corporation. The financial support of the Swedish Foundation for Strategic Environmental Research, MISTRA, is gratefully acknowledged. The work was done within the framework of the Fuel Cell Program.

References

[1] R. O'Hayre, S.W. Cha, W. Colella, F.B. Prinz, Fuel Cell Fundamentals, John Wiley & Sons, New Jersey, 2005.
[2] H.A. Gasteiger, S.S. Kocha, B. Sompalli, F.T. Wagner, Appl. Catal. B: Environ. 56 (2005) 9.
[3] S. Litster, G. McLean, J. Power Sources 130 (2004) 61.
[4] S. Mukerjee, J. Appl. Electrochem. 20 (1990) 537.
[5] W. Sun, B.A. Peppley, K. Karan, Electrochim. Acta 50 (2005) 3359.
[6] D. Song, Q. Wang, Z. Liu, M. Eikerling, Z. Xie, T. Navessin, S. Holdcroft, Electrochim. Acta 50 (2005) 3347.
[7] G. Li, P.G. Pickup, J. Electrochem. Soc. 150 (2003) C745.
[8] E. Antolini, J. Appl. Electrochem. 34 (2004) 563.
[9] H. Ekström, P. Hanarp, M. Gustafsson, E. Fridell, A. Lundblad, G. Lindbergh, J. Electrochem. Soc. 153 (2006) A724.
[10] M. Gustavsson, H. Fredriksson, B. Kasemo, Z. Jusys, J. Kaiser, C. Jun, R.J. Behm, J. Electroanal. Chem. 568 (2004) 371.
[11] P. Hanarp, D.S. Sutherland, J. Gold, B. Kasemo, Colloids, Surf. A: Physicochem. Eng. Aspects 214 (2003) 23.
[12] U.A. Paulus, Z. Veziridis, B. Schnyder, M. Kuhnke, G.G. Scherer, A. Wokaun, J. Electroanal. Chem. 541 (2003) 77.
[13] L. Osterlund, S. Kielbassa, C. Werdinius, B. Kasemo, J. Catal. 215 (2003) 94.
[14] S. Johansson, L. Osterlund, B. Kasemo, J. Catal. 201 (2001) 275.
[15] G.A. Somorjai, M. Yang, Topics Catal. 24 (2003) 61.
[16] J. Libuda, S. Schauermann, M. Laurin, T. Schalow, H. Freund, Monatsh. Chem. 136 (2005) 59.
[17] R. O'Hayre, S.-J. Lee, S.-W. Cha, F.B. Prinz, J. Power Sources 109 (2002) 483.
[18] S.Y. Cha, W.M. Lee, J. Electrochem. Soc. 146 (1999) 4055.
[19] A.T. Haug, R.E. White, J.W. Weidner, W. Huang, S. Shi, T. Stoner, N. Rana, J. Electrochem. Soc. 149 (2002) A280.
[20] T. Nakakubo, M. Shibata, K. Yasuda, J. Electrochem. Soc. 152 (2005) A2316.
[21] D. Gruber, N. Ponath, J. Muller, F. Lindstaedt, J. Power Sources 150 (2005) 67.
[22] Y.K. Xiu, N. Nakagawa, J. Electrochem. Soc. 151 (2004) A1483.
[23] A.F. Gullá, M.S. Saha, R. Allen, S. Mukerjee, Electrochem. Solid State Lett. 8 (2005) A504.
[24] B. Wang, J. Power Sources 152 (2005) 1.
[25] J. Shim, C.-R. Lee, H.-K. Lee, J.-S. Lee, E.J. Cairns, J. Power Sources 102 (2001) 172.
[26] L. Xiong, A. Manthiram, Electrochim. Acta 49 (2004) 4163.

[27] S.V. Mentus, Electrochim. Acta 50 (2005) 3609.
[28] G. Kokkinidis, D. Stoychev, V. Lazarov, A. Papoutsis, A. Milchev, J. Electroanal. Chem. 511 (2001) 20.
[29] K. Tammeveski, M. Arulepp, T. Tenno, C. Ferrater, J. Claret, Electrochim. Acta 42 (1997) 2961.
[30] J. Ihonen, F. Jaouen, G. Lindbergh, G. Sundholm, Electrochim. Acta 46 (2001) 2899.
[31] A.W. Grant, Q.-H. Hu, B. Kasemo, Nanotechnology 15 (2004) 1175.
[32] D.R. Jennison, O. Dulub, W. Hebenstreit, U. Diebold, Surf. Sci. 492 (2001) L677.
[33] S. Lunell, A. Stashans, L. Ojamae, H. Lindstrom, A. Hagfeldt, J. Am. Chem. Soc. 119 (1997) 7374.
[34] T. Navessin, S. Holdcroft, Q. Wang, D. Song, Z. Liu, M. Eikerling, J. Horsfall, K.V. Lovell, J. Electroanal. Chem. 567 (2004) 111.